

## Determination of plasma frequency, damping constant, and size distribution from the complex dielectric function of noble metal nanoparticles

Luis J. Mendoza Herrera, David Muñetón Arboleda, Daniel C. Schinca, and Lucía B. Scaffardi

Citation: *Journal of Applied Physics* **116**, 233105 (2014); doi: 10.1063/1.4904349

View online: <http://dx.doi.org/10.1063/1.4904349>

View Table of Contents: <http://scitation.aip.org/content/aip/journal/jap/116/23?ver=pdfcov>

Published by the [AIP Publishing](#)

---

### Articles you may be interested in

[Extended Maxwell-Garnett-Mie formulation applied to size dispersion of metallic nanoparticles embedded in host liquid matrix](#)

*J. Chem. Phys.* **140**, 044705 (2014); 10.1063/1.4862995

[Photoresponse from noble metal nanoparticles-multi walled carbon nanotube composites](#)

*Appl. Phys. Lett.* **101**, 241113 (2012); 10.1063/1.4771125

[Acoustic oscillations of spherical metallic nanoparticles in dielectric media driven by ultrashort laser pulses](#)

*Low Temp. Phys.* **37**, 329 (2011); 10.1063/1.3592679

[Dependence of the localized surface plasmon resonance of noble metal quasispherical nanoparticles on their crystallinity-related morphologies](#)

*J. Chem. Phys.* **134**, 024507 (2011); 10.1063/1.3523645

[Dielectric function of Cu, Ag, and Au obtained from reflection electron energy loss spectra, optical measurements, and density functional theory](#)

*Appl. Phys. Lett.* **89**, 213106 (2006); 10.1063/1.2397026

---

The advertisement features a dark blue background with a film strip graphic on the left side. The text is centered and reads: 'Not all AFMs are created equal' in orange, 'Asylum Research Cypher™ AFMs' in white, and 'There's no other AFM like Cypher' in orange. At the bottom, the website 'www.AsylumResearch.com/NoOtherAFMLikeIt' is listed in white, and the Oxford Instruments logo is in the bottom right corner with the tagline 'The Business of Science®'.

**Not all AFMs are created equal**  
**Asylum Research Cypher™ AFMs**  
**There's no other AFM like Cypher**

[www.AsylumResearch.com/NoOtherAFMLikeIt](http://www.AsylumResearch.com/NoOtherAFMLikeIt)

**OXFORD**  
INSTRUMENTS  
*The Business of Science®*

# Determination of plasma frequency, damping constant, and size distribution from the complex dielectric function of noble metal nanoparticles

Luis J. Mendoza Herrera,<sup>1</sup> David Muñetón Arboleda,<sup>1</sup> Daniel C. Schinca,<sup>1,2</sup> and Lucía B. Scaffardi<sup>1,2,a)</sup>

<sup>1</sup>Centro de Investigaciones Ópticas (CIOp), (CONICET La Plata-CIC), Argentina

<sup>2</sup>Departamento de Ciencias Básicas, Facultad de Ingeniería, UNLP, Argentina

(Received 3 September 2014; accepted 2 December 2014; published online 19 December 2014)

This paper develops a novel method for simultaneously determining the plasma frequency  $\omega_p$  and the damping constant  $\gamma_{free}$  in the bulk damped oscillator Drude model, based on experimentally measured real and imaginary parts of the metal refractive index in the IR wavelength range, lifting the usual approximation that restricts frequency values to the UV-deep UV region. Our method was applied to gold, silver, and copper, improving the relative uncertainties in the final values for  $\omega_p$  (0.5%–1.6%) and for  $\gamma_{free}$  (3%–8%), which are smaller than those reported in the literature. These small uncertainties in  $\omega_p$  and  $\gamma_{free}$  determination yield a much better fit of the experimental complex dielectric function. For the case of nanoparticles (Nps), a series expansion of the Drude expression (which includes  $\omega_p$  and  $\gamma_{free}$  determined using our method) enables size-dependent dielectric function to be written as the sum of three terms: the experimental bulk dielectric function plus two size corrective terms, one for free electron, and the other for bound-electron contributions. Finally, size distribution of nanometric and subnanometric gold Nps in colloidal suspension was determined through fitting its experimental optical extinction spectrum using Mie theory based on the previously determined dielectric function. Results are compared with size histogram obtained from Transmission Electron Microscopy (TEM). © 2014 AIP Publishing LLC.  
<http://dx.doi.org/10.1063/1.4904349>

## I. INTRODUCTION

Optical properties of metal Nps are especially important when specific applications are studied.<sup>1–12</sup> In a “top-down” approach, these properties can be described by their bulk dielectric function ( $\epsilon$ ), which may be represented as the sum of two terms: one corresponding to the contribution of free electrons based on the metal Drude model (intraband transitions) and the other corresponding to bound electrons (interband transitions). Due to the characteristics of this approach, the influence of each contribution depends on wavelength  $\lambda$ : for sufficiently large wavelengths (small photon energies), free-electron contribution dominates, while for smaller wavelengths (large photon energies), bound-electron contribution is more important.

It is well known that the Drude model assumes that an incoming electromagnetic wave of frequency  $\omega$  forces damped oscillations of the essentially free metal electrons, with a damping constant  $\gamma_{free}$ . The model involves a typical frequency (plasma frequency  $\omega_p$ ) above which the metal reflectivity decreases. To get an approximate expression for the Drude dielectric function, the condition  $\omega \gg \gamma_{free}$  is often used.<sup>13–17</sup> This condition is a valid mathematical inequality that allows obtaining a linear relation between  $\epsilon$  (real) and  $\lambda^2$  from which  $\omega_p$  can be determined. However, for the frequency range imposed by this restriction (UV-deep UV), the dielectric function must be described not only considering intraband transitions (free electrons) but also interband

transitions (bound electrons). It seems reasonable then to find an alternative way to overcome this difficulty by determining these parameters to lift that restriction.

This work is developed in three steps. The first one presents a way to determine  $\omega_p$  and  $\gamma_{free}$  simultaneously, avoiding the approximation  $\omega \gg \gamma_{free}$ , working in the range where Drude model dominates and the influence of bound-electron transitions is negligible. The method is applied to obtain the values of these constants for the cases of gold, silver and copper.

For spherical Nps under 20 nm radii, the full dielectric function becomes size dependent through corrections introduced specifically into  $\gamma_{free}$  and into the bound-electron expression.<sup>18–21</sup> In the second step, the full dielectric function is rewritten considering the size-dependent free-electron contribution as a power series expansion of radius and frequency and a size-dependent term for bound electrons. The final expression, obtained after regrouping, may be reinterpreted as the bulk dielectric function (which is usually measured experimentally as a function of frequency or wavelength) plus size corrective terms for free and bound electrons. This way of writing the full size-dependent dielectric function allows the uncertainty in its determination to be mainly focused on that of the bulk experimental data.

The size-dependent dielectric function is analyzed in the 50–3 nm Nps size range, comparing the real and imaginary parts of the experimental dielectric function with the calculated values. Below 3 nm size, the influence of bound-electron contribution on the complex dielectric function is analyzed.

<sup>a)</sup>Author to whom correspondence should be addressed. Electronic mail: [lucias@ciop.unlp.edu.ar](mailto:lucias@ciop.unlp.edu.ar)

The third step concerns the fit of experimental extinction spectrum of subnanometric gold Nps in colloidal suspension using the size-dependent dielectric function determined with this approach, together with Mie theory. We discuss these results with those obtained by TEM microscopy.

**II. DETERMINATION OF  $\omega_p$  and  $\gamma_{free}$ : BACKGROUND AND RESULTS**

The first approximation to metal dielectric function is based on the so called Drude model, which considers that electrons in a metal are essentially free and can be forced to oscillate when an electromagnetic wave of frequency  $\omega$  is incident upon it. In this case, it can be readily shown<sup>22–26</sup> that metal dielectric function takes the simple form,

$$\epsilon_{free}(\omega) = 1 - \frac{\omega_p^2}{\omega^2 + i\omega\gamma_{free}}, \tag{1}$$

where  $\omega_p$  is the above mentioned plasma frequency and  $\gamma_{free}$  is the damping constant of the electron oscillatory movement, the latter representing the damping of electron oscillation due to different processes: electron-electron collisions, electron-ion collisions, and electron-phonon collisions. These processes are characterized by the mean time between two successive collisions and are taken into account altogether in the value of  $\gamma_{free}$ , although they cannot be specifically separated within the parameterization of the bulk dielectric function.

As a general approach, these two parameters may be determined by fitting the experimental complex dielectric function spectrum using a least-square regression over the spectral range without apparent interband transition contributions. However, this method requires a guess for this interband-free spectral range, a fact that may lead to a poor accuracy in the determination of  $\omega_p$  and  $\gamma_{free}$ .

On the other hand, many authors<sup>13–17</sup> use the condition  $\omega \gg \gamma_{free}$  to obtain a very simple approximate expression for the dielectric function that yield a linear relation between the real part of  $\epsilon_{free}$  and the square of the wavelength. From the slope of this relation,  $\omega_p$  can be determined. A similar situation occurs for the imaginary part of  $\epsilon_{free}$ , from which  $\gamma_{free}$  can be determined. However, as mentioned in Sec. I, the wavelength range imposed by the condition  $\omega \gg \gamma_{free}$  lies in the UV-deep UV, where bound-electron contribution to the dielectric function of noble metals such as gold, silver and copper is not negligible.

To overcome the limiting condition mentioned above, it is necessary to find a method that may yield information about the wavelength range where the Drude model is satisfied and its parameters determined without any “*a priori*” restriction. If the real ( $\epsilon'$ ) and imaginary ( $\epsilon''$ ) parts of Eq. (1) are written separately, it is possible to obtain two different linear relationships between them, as shown

$$\omega\epsilon''(\omega) = \gamma_{free}(1 - \epsilon'(\omega)), \tag{2}$$

$$\omega^2[(\epsilon''(\omega))^2 + (1 - \epsilon'(\omega))^2] = \omega_p^2(1 - \epsilon'(\omega)). \tag{3}$$

From the slopes of these linear plots with zero ordinate crossing,  $\gamma_{free}$  and  $\omega_p^2$  can be determined without using any restriction on the frequency (wavelength) range. Using the experimental values for the complex refractive index ( $n + ik$ ) reported by Ref. 13 in the range 750–2000 nm, the real and imaginary parts of the dielectric function may be derived from the relations  $\epsilon'(\lambda) = n(\lambda)^2 - k(\lambda)^2$  and  $\epsilon''(\lambda) = 2n(\lambda)k(\lambda)$ . Introducing these values into Eqs. (2) and (3) for the different wavelengths given in Ref. 13, it is possible to plot those relations. Figures 1(a), 1(b), and 1(c) show these plots for gold, silver and copper Nps, respectively. Full squares correspond to data obtained from Eq. (3) (left ordinate axis) and hollow circles to data from Eq. (2)

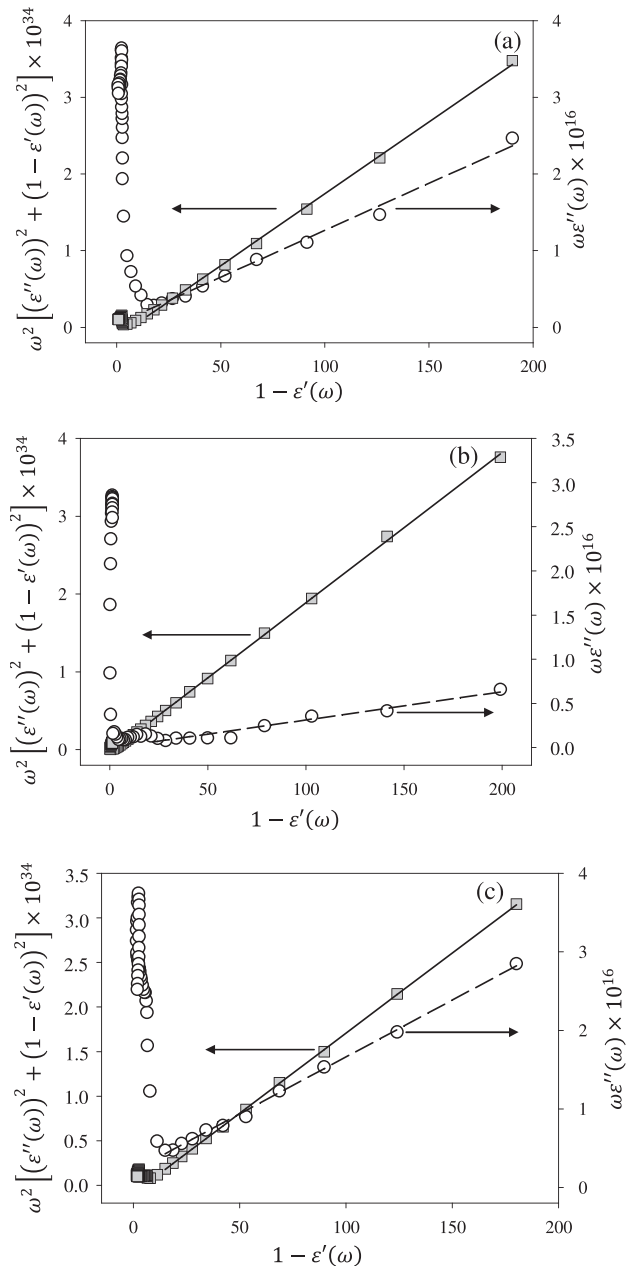


FIG. 1. Plot of Eqs. (2) and (3) for (a) gold, (b) silver and (c) copper. Linear regression fit the data for the wavelength range where the dielectric function can be described purely by the Drude model. Values for  $\epsilon'$  and  $\epsilon''$  are taken from Ref. 13. The slopes of the linear regressions yield the values for  $\omega_p^2$  (full line) and  $\gamma_{free}$  (dashed line).

(right ordinate axis). For each curve, it can be readily seen that it is possible to fit a determined range of values with a linear regression with zero ordinate crossing. The wavelength range for which these regressions fit the data corresponds to the region where the influence of interband transitions is negligible, i.e., where the metal satisfies the Drude model. The slope of the full squares linear regression (full line) allows determining  $\omega_p^2$ , while the slope of the linear regression for the hollow circles (dashed line) allows determining  $\gamma_{free}$ . It can also be seen that the fits are linear for a range of frequency values that satisfy the condition  $1 - \epsilon'(\omega) > 14$  for gold,  $1 - \epsilon'(\omega) > 21$  for silver, and  $1 - \epsilon'(\omega) > 15$  for copper. For the three cases, the smaller wavelength that satisfies these conditions is about 660 nm. Since the wavelength for which a metal may be considered Drude-like is not known *a priori*, the approach presented above has the advantage of clearly separating the spectral regions where free or bound-electron contributions are dominant. This separation is given by the corresponding wavelength value from which the plots in Figure 1 become linear (free-electron contribution). Out of this region, the data cannot be fitted by a linear regression, suggesting that interband transitions contribution is not negligible.

Determined values of  $\omega_p$  and  $\gamma_{free}$ , including their uncertainties, are summarized in Table I for the three analyzed metals together with the values reported in Ref. 13. The uncertainties of the parameters determined in this work are in the range 0.5%–1.6% for  $\omega_p$  and 3%–8% for  $\gamma_{free}$ , which are equal to or smaller than those reported in Ref. 13, where the above mentioned frequency restriction was used.

With the values of  $\omega_p$  and  $\gamma_{free}$  determined in this work, the real and imaginary parts of Eq. (1) can be plotted for the whole wavelength range between 200 nm and 2000 nm.<sup>13</sup> Figure 2(a) shows this plot for gold. It can be seen that these curves fit reasonably well the real (full squares) and imaginary (hollow circles) experimental data for wavelengths larger than about 750 nm, where free-electron contribution dominates. In particular, the imaginary part is reliably fitted down to about 750 nm. In the short wavelength range, the fit is not so good, since the bound-electron contributions are stronger.

Figure 2(b) shows the free-electron contribution for silver. It can be seen that the general features are very similar to those for gold, except that the imaginary part may be reliably reproduced down to about 300 nm. This is consistent with the fact that onset for interband transitions in silver lies in the UV region.<sup>23</sup> Finally, Figure 2(c) shows the behavior

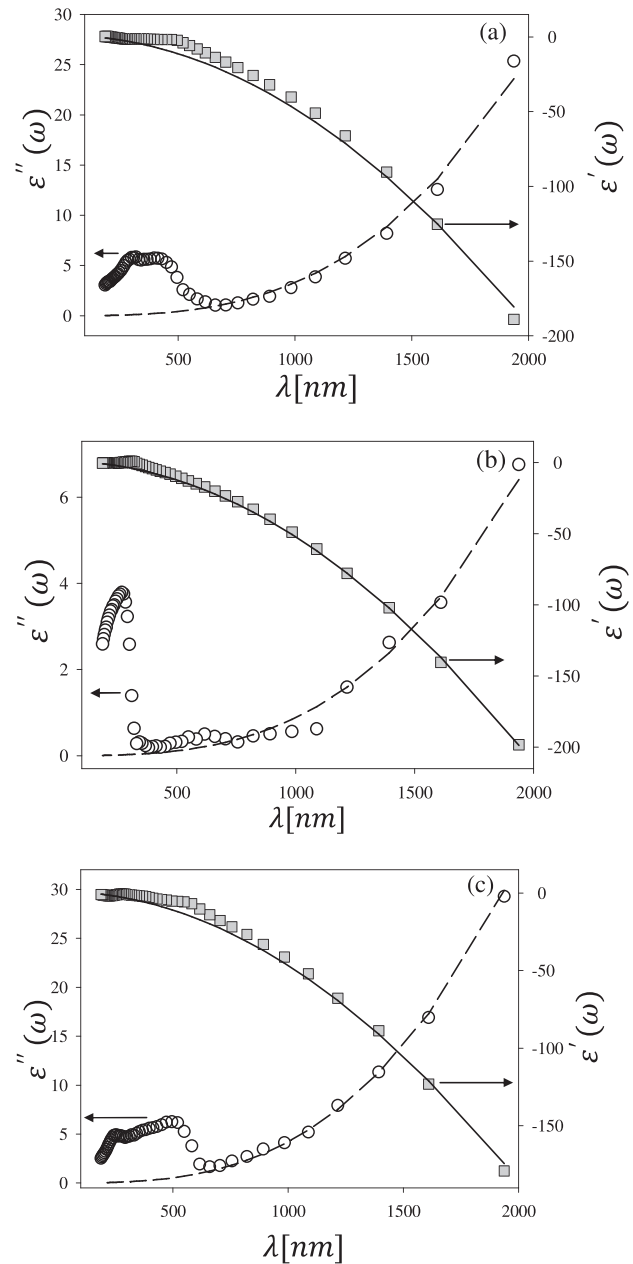


FIG. 2. Real (full line) and imaginary (dashed line) parts of free- electron contribution for (a) gold, (b) silver and (c) copper given by Eq. (1) using  $\omega_p$  and  $\gamma_{free}$  values calculated in this work. Grey squares and hollow circles represent the real and imaginary parts of experimental bulk dielectric function, respectively. Right and left vertical axes scale the real and imaginary parts, respectively.

TABLE I. Values of  $\omega_p$  and  $\gamma_{free}$  determined by the slope of a linear regression of Eqs. (2) and (3).

Metal	$\omega_p$ [1/s]	Reference	$\gamma_{free}$ [1/s]
Gold	$(1.323 \pm 0.021) \times 10^{16}$	(This work)	$(1.26 \pm 0.04) \times 10^{14}$
	$(1.370 \pm 0.055) \times 10^{16}$	13	$(1.07 \pm 0.17) \times 10^{14}$
Silver	$(1.375 \pm 0.007) \times 10^{16}$	(This work)	$(3.12 \pm 0.25) \times 10^{13}$
	$(1.393 \pm 0.007) \times 10^{16}$	13	$(3.22 \pm 1.24) \times 10^{13}$
Copper	$(1.307 \pm 0.014) \times 10^{16}$	(This work)	$(1.66 \pm 0.09) \times 10^{14}$
	$(1.344 \pm 0.054) \times 10^{16}$	13	$(1.45 \pm 0.14) \times 10^{14}$

of complex free-electron contribution for copper, which is similar to the case of gold, showing a good agreement for wavelengths larger than about 700 nm.

To model the experimental bulk dielectric function at short wavelengths (smaller than 700 nm) it is necessary to consider bound-electron contribution which is due to *d-sp* interband transitions, not considered in the Drude approach. Besides, when Nps of several tens of nanometers in size are considered, a size-dependent term in the expression of the dielectric function must be introduced both for free and bound- electron contributions. These issues will be addressed next.

### III. SIZE-DEPENDENT DIELECTRIC FUNCTION

As mentioned in a previous paragraph, the bulk metal dielectric function may be considered as an additive contribution of free and bound electrons. The former can be described with the well known Drude model, while the latter contribution may be suitably described by a Lorentz-type term that takes into account interband transitions. With these assumptions, general bulk dielectric function can be written as<sup>22–26</sup>

$$\varepsilon_{bulk}(\omega) = 1 - \frac{\omega_p^2}{\omega^2 + i\omega\gamma_{free}} + \sum_j \frac{\omega_{pj}^2}{\omega_j^2 - \omega^2 + \gamma_j^2 - 2i\gamma_j\omega}, \quad (4)$$

where  $\gamma_{free}$  and  $\omega_p$  are determined using the approach described in Sec. II (numerically shown in Table I),  $\omega_{pj}$ ,  $\omega_j$ , and  $1/\gamma_j$  are the plasma frequency, the central frequency and the lifetime of the  $j$ -th interband transition, respectively. The values of the complex bulk dielectric function  $\varepsilon_{bulk}(\omega)$  are taken from experimental measurements given in Ref. 13. Since the metals studied in this work satisfy the Random Phase Approximation (RPA),<sup>18–21,27</sup> the expression for bound-electron contribution can be written as an integral over a continuum of interband transitions. So, expression (4) may be rewritten as

$$\varepsilon_{bulk}(\omega) = 1 - \frac{\omega_p^2}{\omega^2 + i\omega\gamma_{free}} + K_b \int_{\omega_g}^{\infty} \frac{\sqrt{x - \omega_g}}{x} [1 - F(x, T)] \times \frac{dx}{x^2 - \omega^2 + \gamma_{bound}^2 - 2i\gamma_{bound}\omega}, \quad (5)$$

where  $E_g = \hbar\omega_g$  is the gap energy,  $F(x, T)$  is the Fermi distribution for electrons of energy  $\hbar x$  and temperature  $T$ ,  $\gamma_{bound}$  stands for the bound-electron damping constant, and  $K_b$  is a proportionality factor, with units of  $[s^{-1}]^{3/2}$ . Notice that the last term in Eq. (5) represents an explicit description of bound-electron contribution in terms of electron oscillation parameters  $\gamma_{bound}$ ,  $\omega_g$ , and  $E_F$  within  $F(x, T)$ . Values of  $\gamma_{bound}$ ,  $\omega_g$ ,  $F(x, T)$ , and  $K_b$  for gold, copper, and silver were determined in our previous works.<sup>18–21</sup>

For spherical Nps under 20 nm radius,<sup>22</sup> electron collisions with the particle boundary reduce the mean free path, increasing the collision frequency. In a “top-down” description of size effects, this fact may be taken into account by a modification of the free electron damping constant in the form  $\gamma_{size}(R) = \gamma_{free} + C \frac{v_F}{R}$ ,<sup>22,28</sup> where  $v_F$  is the Fermi velocity and  $C$  is a constant that depends on the material and on the carrier scattering at the particle wall. For noble metals, it has a value about 0.8.<sup>28</sup>

For Nps an order of magnitude smaller, the parameter  $K_b$  in equation (5) must also be corrected as  $K_{size} = K_b(1 - e^{-R/R_0})$ , where  $R_0$  is a scale factor that represents the range for which the density of states can be considered to reach the value of the bulk.<sup>18–21</sup> With the above corrections, the full size-dependent dielectric function for spherical Nps can be written as a function of frequency and radius as

$$\varepsilon(\omega, R) = 1 - \frac{\omega_p^2}{\omega^2 + i\omega\gamma_{free} + i\omega C \frac{v_F}{R}} + K_b(1 - e^{-R/R_0}) \int_{\omega_g}^{\infty} \frac{\sqrt{x - \omega_g}}{x} [1 - F(x, T)] \times \frac{dx}{x^2 - \omega^2 + \gamma_{bound}^2 - 2i\gamma_{bound}\omega}. \quad (6)$$

At this point, we consider a power series expansion of the second term of Eq. (6) in the form

$$\frac{\omega_p^2}{\omega^2 + i\omega\gamma_{free} + i\omega C \frac{v_F}{R}} = \omega_p^2 \sum_{n=0}^{\infty} (-1)^n \frac{\left(\frac{i\omega C v_F}{R}\right)^n}{(\omega^2 + i\omega\gamma_{free})^{n+1}}, \quad (7)$$

where convergence criterion yields the inequality  $\omega > \gamma_{bulk} + C \frac{v_F}{R}$ , that is for  $\omega > \gamma_{size}(R)$  (see Appendix). This condition imposes the maximum wavelength limit for which the above expansion method can be used to describe the free-electron contribution to dielectric function.

Introducing this series expansion into Eq. (6),  $\varepsilon(\omega, R)$  may be rewritten as

$$\varepsilon(\omega, R) = 1 - \omega_p^2 \sum_{n=0}^{\infty} (-1)^n \frac{\left(\frac{i\omega C v_F}{R}\right)^n}{(\omega^2 + i\omega\gamma_{free})^{n+1}} + K_b \int_{\omega_g}^{\infty} \frac{\sqrt{x - \omega_g}}{x} [1 - F(x, T)] \times \frac{dx}{x^2 - \omega^2 + \gamma_{bound}^2 - 2i\gamma_{bound}\omega} - K_b e^{-\frac{R}{R_0}} \int_{\omega_g}^{\infty} \frac{\sqrt{x - \omega_g}}{x} [1 - F(x, T)] \times \frac{dx}{x^2 - \omega^2 + \gamma_{bound}^2 - 2i\gamma_{bound}\omega}.$$

Making a suitable regrouping of terms, the size-dependent dielectric function can be written in terms of the bulk dielectric function as

$$\varepsilon(\omega, R) = \varepsilon_{bulk}(\omega) + \Delta\varepsilon_{free}(\omega, R) + \Delta\varepsilon_{bound}(\omega, R), \quad (8)$$

where

$$\varepsilon_{bulk}(\omega) = 1 - \frac{\omega_p^2}{(\omega^2 + i\omega\gamma_{free})} + K_b \int_{\omega_g}^{\infty} \frac{\sqrt{x - \omega_g}}{x} [1 - F(x, T)] \times \frac{dx}{x^2 - \omega^2 + \gamma_{bound}^2 - 2i\gamma_{bound}\omega}, \quad (9)$$

$$\Delta\varepsilon_{free}(\omega, R) = -\omega_p^2 \sum_{n=1}^{\infty} (-1)^n \frac{\left(\frac{i\omega C v_F}{R}\right)^n}{(\omega^2 + i\omega\gamma_{free})^{n+1}}, \quad (10)$$

$$\Delta\epsilon_{bound}(\omega, R) = -K_b e^{-R/R_0} \int_{\omega_g}^{\infty} \frac{\sqrt{x - \omega_g}}{x} [1 - F(x, T)] dx \times \frac{1}{x^2 - \omega^2 + \gamma_{bound}^2 - 2i\gamma_{bound}\omega}. \quad (11)$$

The expressions for  $\Delta\epsilon_{free}(\omega, R)$  and  $\Delta\epsilon_{bound}(\omega, R)$  in Eq. (8) may be regarded as size-dependent corrective terms to the experimental bulk dielectric function  $\epsilon_{bulk}(\omega)$  given, for example, by Ref. 13. Equations (8)–(11) allow determining the size dielectric function in terms of wavelength for gold, copper and silver using values of  $\omega_p$  and  $\gamma_{free}$  shown in Table I.

Regarding the number of terms to be used in the series expansion of  $\Delta\epsilon_{free}(\omega, R)$ , it is clear from Eq. (10) that it depends on wavelength (frequency) and radius. For gold Nps with radii  $R \geq 9$  nm, the full size-dependent dielectric function (Eq. (6)) was compared with expression (8) taking only one term of the series expansion (Eq. (10)). The difference between both theoretical calculated values (using  $\omega_p$  and  $\gamma_{free}$  parameters determined in Sec. II) is less than 7% in the wavelength range 200–2000 nm. For these calculations, the following values determined in Ref. 29 were used:  $\omega_g = 3.2 \times 10^{15} \text{ s}^{-1}$ ,  $\gamma_{bound} = 2.4 \times 10^{14} \text{ s}^{-1}$ ,  $K_b = 2.3 \times 10^{24} [\text{s}^{-1}]^{3/2}$ ,  $E_F = 2.5 \text{ eV}$

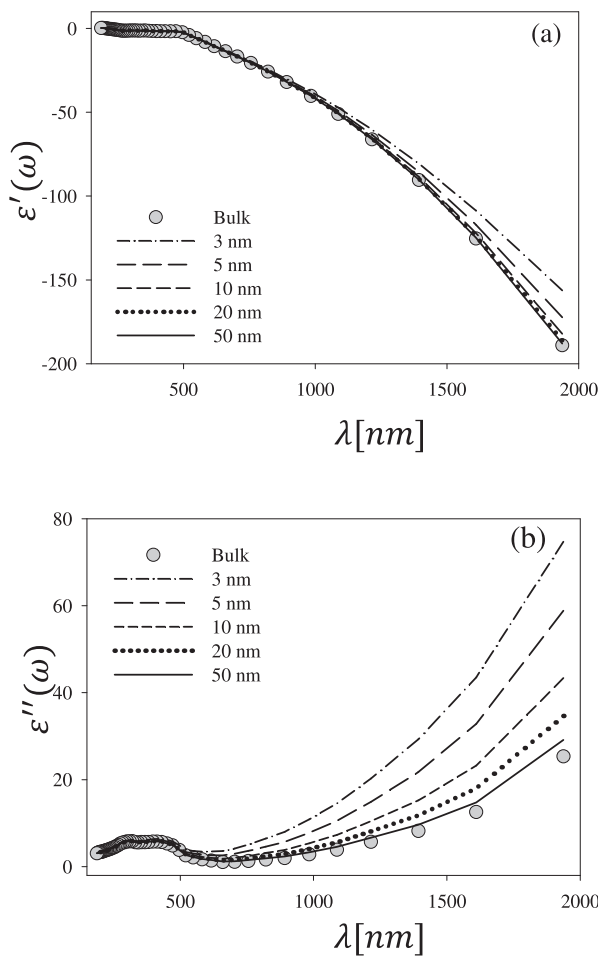


FIG. 3. Theoretical values for real (a) and imaginary (b) parts of gold dielectric function as a function of wavelength for different radii. Experimental bulk values are represented by grey full circles.

and  $v_F = 14.1 \times 10^{14} \frac{\text{nm}}{\text{s}}$ . Values of  $\omega_p$  and  $\gamma_{free}$  are those calculated in this work and shown in Table I.

Figure 3 shows the real (a) and imaginary (b) parts of the dielectric function for gold spherical Nps of different sizes. It can be seen in panel (a) that for  $R = 50$  nm,  $\epsilon'$  coincides with the experimental bulk values (grey dots). As the size gets smaller (for example, 3 nm), the real dielectric function departs from bulk values for wavelengths larger than 800 nm. This behavior is due to the larger influence of free electron corrective term  $\Delta\epsilon_{free}(\omega, R)$  with respect to the bound-electron contribution corrective term  $\Delta\epsilon_{bound}(\omega, R)$ . The imaginary part, instead, departs from bulk behavior from about 600 nm onwards, as seen in panel (b).

To analyze the influence of  $\Delta\epsilon_{bound}(\omega, R)$ , Eq. (8) is plotted in Figure 4 with and without this term for the case of gold. Panels (a) and (b) show theoretical calculation of real and imaginary parts of the dielectric function in the wavelength range 200–800 nm, comparing their behavior for different radii. It is clearly observed that, for radii larger than 2 nm, there is no difference in considering or not the bound-electron corrective term, since the two curves (grey and black triangles) are superimposed. However, for decreasing radii, the difference gets larger. For example, for 1 nm and

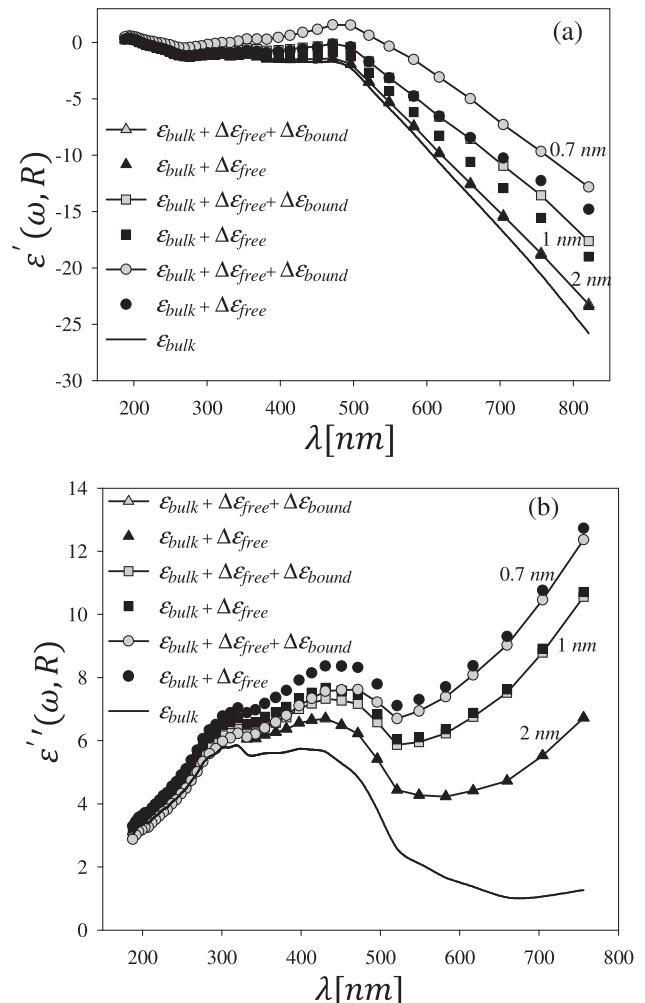


FIG. 4. comparison of real part (a) and imaginary part (b) of the full gold Nps dielectric function for the case of small radii calculated using Eq. (8) with and without bound-electron corrective term.

0.7 nm radius, there is a noticeable difference between the curves that include or not  $\Delta\varepsilon_{bound}(\omega, R)$  for wavelengths shorter than 800 nm. As a general conclusion it can be said that the bound-electron corrective term is important for sizes smaller than 2 nm due to the fact that the exponential factor in equation (11) saturates for  $R \geq 2$  nm. For  $R > 2$  nm radii only free-electron corrective term is relevant.

For comparison purposes, the real and imaginary parts of the bulk dielectric function are plotted in full line in the corresponding panels.

#### IV. EXTINCTION SPECTRUM OF SUBNANOMETRIC GOLD NANOPARTICLES

An interesting application of the above method is in nanoparticle sizing using optical spectroscopic analysis. Since gold is one of the most studied metals for nanostructure forming, we chose gold Nps which were synthesized using the reverse micelle method in water–hydrocarbon phases and isolated with a stabilizer following the procedure described in Ref. 18. Particles were capped with a stabilization agent to avoid agglomeration in organic solvents. Reverse micelle method tends to create small spherical Nps, typically under 10 nm.

Extinction spectra of gold nanoparticles' suspension dispersed in heptane, appropriately diluted to avoid multiple scattering effects, were recorded between 300 and 1100 nm. A typical spectrum for a gold sample is shown in Figure 5. The experimental data (grey circles) are fitted considering the optical extinction response of small spherical Nps (compared with wavelength) as described by Mie theory.<sup>22</sup> The extinction cross section  $C_{ext}$  is a function of the polarizability which, in turn, depends on the metal dielectric function  $\varepsilon(\omega, R)$  (calculated through Eq. (8)), and the dielectric function of the surrounding medium  $\varepsilon_m(\omega)$ , which was evaluated using Sellmeier's equations. A parameter related with the extinction cross section, which is often used for spectra plotting purposes, is the so called extinction coefficient defined as  $Q_{ext} = \frac{C_{ext}}{\pi R^2}$ .

Best fit was obtained considering a log-normal size distribution represented by the expression:

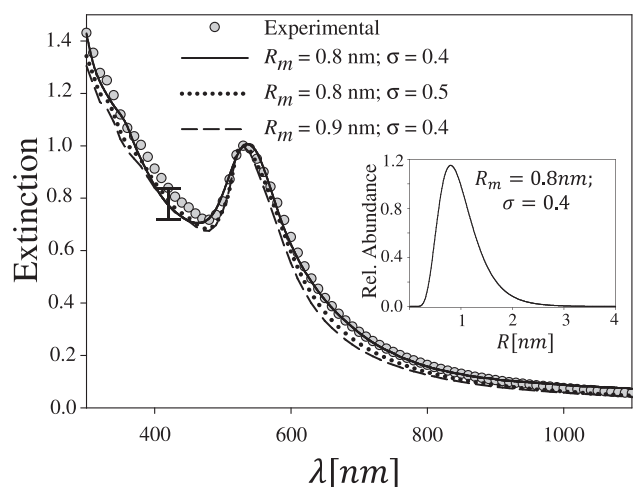


FIG. 5. Experimental extinction spectrum of small gold nanoparticles (grey dots) in n-heptane. Best fit (full line) for a log-normal size distribution (inset). Dotted and dashed lines correspond to out-of-optimum fit.

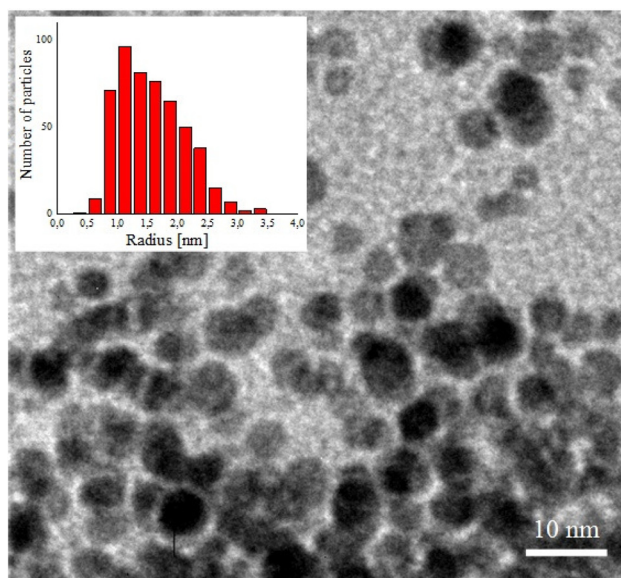


FIG. 6. TEM image of gold Nps in colloidal suspension. Inset shows the size distribution histogram.

$$f(R) = \frac{1}{R\sigma\sqrt{2\pi}} \exp\left(-\frac{(\ln R - \mu)^2}{2\sigma^2}\right),$$

where  $f(R)$  is the percentage of particles of radius  $R$ , and  $\mu$  and  $\sigma$  are the mean and standard deviation of the distribution, respectively. The expected value  $R_m$  of the radius is given by  $R_m = \exp(\mu - \sigma^2)$ . Full line in Figure 5 corresponds to the best fit for a size distribution with  $R_m = 0.8$  nm and  $\sigma = 0.4$  (inset). Dotted and dashed lines represent fits for  $R_m$  and  $\sigma$  values slightly different from those considered optimum. It can be seen that even for these small changes there is an observable difference in the full fit of the spectrum, a fact that shows the sensitivity of this sizing method. The parameters used for the fitting of the experimental spectrum in Figure 5 are those mentioned in Sec. III, following Eq. (11).

The theoretical curve that fits the extinction spectrum is based on experimental data of complex refractive index using spectroscopic ellipsometry. These measurements are dependent on film topology, grain size and temperature, which render a dispersion of about 10% in the values of the experimental complex refractive index. This dispersion yields a 5% error in the theoretical curves. In the wavelength range 400 to 500 nm in Figure 5, the experimental values of extinction spectrum fall within these error bars, suggesting a very good agreement between experimental and theoretical calculation.

Finally, Figure 6 shows a TEM picture of gold Nps present in the studied colloidal suspension, where the spherical shape of the particles is clearly seen. The shape of the size distribution histogram (inset) is very similar to a log-normal curve with an expected radius of about 1 nm and extending up to 3.5 nm in agreement with the results derived from extinction spectroscopy. Direct TEM size measurements were made over more than 550 particles, while optical extinction measurements were made over about  $10^{15}$  Nps, as estimated by Lambert-Beer law. In spite of the difference in sampling amount, the results obtained by these two techniques are in good agreement.

## V. CONCLUSIONS

We have introduced a new approach to determine simultaneously the Drude parameters  $\omega_p$  and  $\gamma_{free}$  to describe gold, silver, and copper. The method is based on the determination of the slope of linear fits of relations of  $\varepsilon'(\omega)$  and  $\varepsilon''(\omega)$  as a function of  $1 - \varepsilon'(\omega)$  for large wavelengths, without using the approximation  $\omega \gg \gamma_{free}$ , often used in the literature. The relative uncertainties obtained with our method (0.5%–1.6% for  $\omega_p$  and 3%–8% for  $\gamma_{free}$ ) improves those found in the literature. Knowledge of these parameters is important to describe the optical properties of nanosized materials in a “top-down” approach. Besides, the method presented in this paper has the advantage of clearly separating the spectral regions where free (Drude-like) or bound-electron contributions are dominant.

In a second step, these values were introduced in the expression of the full complex dielectric function considering a series expansion of the free-electron contribution. Regrouping terms allows rewriting the general size-dependent dielectric function as the sum of three terms: the experimental bulk dielectric function plus a size corrective term for free electrons  $\Delta\varepsilon_{free}(\omega, R)$  and a size corrective term for bound-electron contribution  $\Delta\varepsilon_{bound}(\omega, R)$ , written taking into account the RPA approximation.

The influence of the corrective term  $\Delta\varepsilon_{free}(\omega, R)$  is important for radii below 10 nm. On the other hand, the influence of  $\Delta\varepsilon_{bound}(\omega, R)$  is noticeable for radii below 2 nm. The main advantage of the series expansion approach used in this work is that the total size-dependent dielectric function may be written as the bulk function plus two size corrective terms. Since this method avoids fitting the bulk values, the uncertainty in the dielectric function is mainly due to that obtained during the experimental bulk data determination.

Finally, taking into account the full expression for the size-dependent dielectric function, the optical extinction spectrum of gold Nps prepared by reverse micelle method was fitted with a log-normal size distribution centered at 0.8 nm radius, obtaining a very good agreement with the experimental data in the wavelength range 300–1000 nm.

## ACKNOWLEDGMENTS

This work was granted by PIP 0394, PME2006-00018 and 11/I151 Facultad de Ingeniería of Universidad Nacional de La Plata (UNLP), Argentina. D. C. Schinca is member of Comisión de Investigaciones Científicas de la Provincia de Buenos Aires (CIC). L. B. Scaffardi, is researcher of CONICET. L J Mendoza Herrera and D Muñetón Arboleda are Doctoral students of UNLP and fellows of CONICET, Argentina.

## APPENDIX: CONVERGENCE CONDITION FOR THE SERIES EXPANSION IN EQ. (7)

In this Appendix, we derive the convergence condition for the series expansion in Eq. (7),

$$\frac{\omega_p^2}{\omega^2 + i\omega\gamma_{free} + i\omega C \frac{v_F}{R}} = \omega_p^2 \sum_{n=0}^{\infty} (-1)^n \frac{\left(\frac{i\omega C v_F}{R}\right)^n}{(\omega^2 + i\omega\gamma_{free})^{n+1}}. \quad (\text{A1})$$

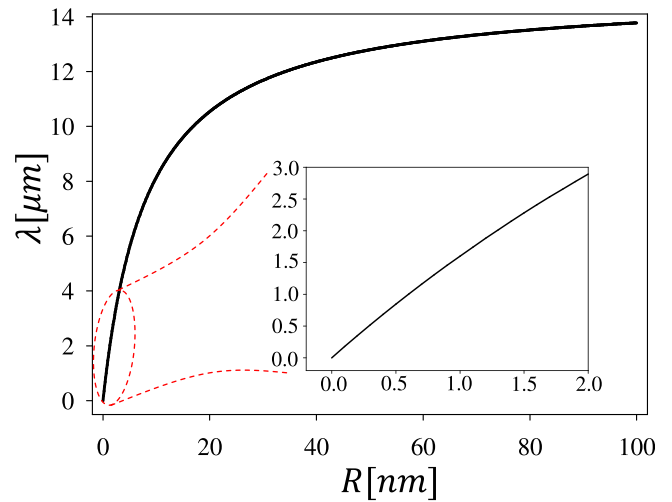


FIG. 7. Maximum wavelength value for which the series in Eq. (A1) converges, as a function of Np radius. Gold dielectric function was taken from Johnson and Christy and  $\omega_p$  and  $\gamma_{free}$  from our calculated values.

This expression was obtained from the general Newton binomial expansion of the form  $(a + b)^{-1}$ , where  $a = \omega^2 + i\omega\gamma_{free}$  and  $b = i\omega C v_F / R$ . Considering  $M = \omega^2$  and  $N = \omega(\gamma_{free} + C v_F / R)$  then

$$(a + b)^{-1} = \frac{1}{M^2 + N^2} (M - iN). \quad (\text{A2})$$

For the convergence of Newton binomial series expansion of  $\frac{1}{M^2 + N^2}$ , the condition  $N^2 < M^2$  must be satisfied. Accordance with the previous definitions, this relation yields

$$\left(\omega\gamma_{free} + \frac{C\omega v_F}{R}\right)^2 < (\omega^2)^2 \quad \text{or} \quad \gamma_{free} + \frac{C v_F}{R} < \omega. \quad (\text{A3})$$

The left member in the Eq. (A3) is the definition of the size-corrected damping constant of the free electrons contribution, so (A3) can be rewritten as  $\omega > \gamma_{size}(R)$ , or as a function of wavelength

$$\lambda < \frac{2\pi c}{\gamma_{size}(R)}. \quad (\text{A4})$$

Equation (A4) indicates the maximum wavelength value for which (for a given radius) the expansion of (A1) converges. Figure 7 plots this relation for the case of gold.

<sup>1</sup>D. Huang, F. Liao, S. Molesa, D. Redinger, and V. Subramanian, “Plastic-compatible low resistance printable gold nanoparticle conductors for flexible electronics,” *J. Electrochem. Soc.* **150**, G412–417 (2003).

<sup>2</sup>T. Stuchinskaya, M. Moreno, M. J. Cook, D. R. Edwards, and D. A. Russell, “Targeted photodynamic therapy of breast cancer cells using antibody–phthalocyanine–gold nanoparticle conjugates,” *Photochem. Photobiol. Sci.* **10**, 822–831 (2011).

<sup>3</sup>S. D. Brown, P. Nativo, J.-A. Smith, D. Stirling, P. R. Edwards, B. Venugopal, D. J. Flint, J. A. Plumb, D. Graham, and N. J. Wheate, “Gold nanoparticles for the improved anticancer drug delivery of the active component of oxaliplatin,” *J. Am. Chem. Soc.* **132**, 4678–4684 (2010).

<sup>4</sup>M. E. Ali, U. Hashim, S. Mustafa, Y. B. Che Man, and Kh. N. Islam, “Gold nanoparticle sensor for the visual detection of pork adulteration in meatball formulation,” *J. Nanomater.* **2012**, 103607 (2012).

- <sup>5</sup>S. D. Perrault and W. C. W. Chan, "In vivo assembly of nanoparticle components to improve targeted cancer imaging," *Proc. Nat. Acad. Sci. USA* **107**, 11194–11199 (2010).
- <sup>6</sup>G. Peng, U. Tisch, O. Adams, M. Hakim, N. Shehada, Y. Y. Broza, S. Billan, R. Abdah-Bortnyak, A. Kuten, and H. Haick, "Diagnosing lung cancer in exhaled breath using gold nanoparticles," *Nature Nanotechnol.* **4**, 669–673 (2009).
- <sup>7</sup>D. T. Thompson, "Using gold nanoparticles for catalysis," *Nano Today* **2**, 40–43 (2007).
- <sup>8</sup>W. R. Li, X. B. Xie, Q. S. Shi, H. Y. Zeng, Y. S. Ou-Yang, and Y. B. Chen, "Antibacterial activity and mechanism of silver nanoparticles on *Escherichia coli*," *Appl. Microbiol. Biotechnol.* **85**(4), 1115–1122 (2010).
- <sup>9</sup>N. Lubick, "Nanosilver toxicity: ions, nanoparticles-or both?," *Environ. Sci. Technol.* **42**(23), 8617 (2008).
- <sup>10</sup>L. W. Guang, J. J. Huan, Y. Z. Xiao, M. D. Yu, and J. L. Zai, "Novel switchable sensor for phosphate based on the distance-dependant fluorescence coupling of cysteine-capped cadmium sulfide quantum dots and silver nanoparticles," *Analyst* **138**, 2000–2006 (2013).
- <sup>11</sup>W. Qi and Y. Yanbin, "Nonenzymatic sensor for hydrogen peroxide based on the electrodeposition of silver nanoparticles on poly(ionic liquid)-stabilized graphene sheets," *Microchim. Acta* **180**(3–4), 261–268 (2013).
- <sup>12</sup>F. C. Meunier, "Mixing copper nanoparticles and ZnO nanocrystals: A route towards understanding the hydrogenation of CO<sub>2</sub> to methanol?," *Angew. Chem. Int. Ed.* **50**, 4053–4054 (2011).
- <sup>13</sup>P. B. Johnson and R. W. Christy, "Optical constants of the noble metals," *Phys. Rev. B* **6**, 4370–4379 (1972).
- <sup>14</sup>U. Kreibig and C. V. Fragstein, "The limitation of electron mean free path in small silver particles," *Z. Phys.* **224**, 307–323 (1969).
- <sup>15</sup>P. B. Johnson and R. W. Christy, "Optical constants of transition metals: Ti, V, Cr, Mn, Fe, Co, Ni and Pd," *Phys. Rev. B* **9**, 5056 (1974).
- <sup>16</sup>B. T. Draine and B. Hensley, "Magnetic nanoparticles in the interstellar medium: emission spectrum and polarization," *Astrophys. J.* **765**, 159 (2013).
- <sup>17</sup>S. Norrman, T. Andersson, C. G. Granqvist, and O. Hunderi, "Optical absorption in discontinuous gold films," *Solid State Commun.* **23**(4), 261–265 (1977).
- <sup>18</sup>L. B. Scaffardi and J. O. Tocho, "Size dependence of refractive index of gold nanoparticles," *Nanotechnology* **17**(5), 1309–1315 (2006).
- <sup>19</sup>J. M. J. Santillán, F. A. Videla, M. B. Fernández van Raap, D. C. Schinca, and L. B. Scaffardi, "Size-dependent Cu dielectric function for plasmon spectroscopy: Characterization of colloidal suspension generated by fs laser ablation," *J. Appl. Phys.* **112**, 054319-1–054319-8 (2012).
- <sup>20</sup>J. M. J. Santillán, F. A. Videla, M. B. Fernández van Raap, D. Muraca, L. B. Scaffardi, and D. C. Schinca, "Influence of size-corrected bound-electron contribution on nanometric silver dielectric function. Sizing through optical extinction spectroscopy," *J. Phys. D: Appl. Phys.* **46**(43), 435301–11 (2013).
- <sup>21</sup>J. M. J. Santillán, F. A. Videla, M. B. Fernández van Raap, D. C. Schinca, and L. B. Scaffardi, "Analysis of the structure, configuration and sizing of Cu and Cu oxide nanoparticles generated by fs laser ablation of solid target in liquids," *J. Appl. Phys.* **113**, 134305 (2013).
- <sup>22</sup>C. F. Bohren and D. R. Huffman, *Absorption and Scattering of Light by Small Particles* (John Wiley & Sons New York, 1998).
- <sup>23</sup>H. Ehrenreich and H. R. Philipp, "Optical properties of Ag and Cu," *Phys. Rev.* **128**(4), 1622–1629 (1962).
- <sup>24</sup>M. Fox, *Optical Properties of Solids* (Oxford University Press, Oxford, 2011).
- <sup>25</sup>R. W. Boyd, *Nonlinear Optics* (Elsevier, London, 2000).
- <sup>26</sup>C. Kittel, *Quantum Theory of Solids* (John Wiley & Sons New York, 1987).
- <sup>27</sup>J. Bigot, J. Merle, O. Cregut, and A. Daunois, "Electron dynamics in copper metallic nanoparticles probed with femtosecond optical pulses," *Phys. Rev. Lett.* **75**(25) 4702–4705 (1995).
- <sup>28</sup>U. Kreibig and M. Vollmer, *Optical Properties of Metal Clusters* (Springer-Verlag, Berlin, 1995).
- <sup>29</sup>B. Scaffardi Lucía, C. Schinca Daniel, M. Lester, A. Videla Fabián, M. J. Santillán Jesica, and M. Abraham Ekeroth Ricardo, *Size-Dependent Optical Properties of Metallic Nanostructures in VU-VIS and Photoluminescence Spectroscopy for Nanomaterials Characterization*, edited by C. S. S. R. Kumar (Springer-Verlag, Berlin, 2013), pp. 179–223.